The collapse of Io's primary atmosphere in Jupiter eclipse

Constantine Tsang, John Spencer, Emmanuel Lellouch, Miguel Lopez-Valverde, Matthew Richter

AGU PUBLICATIONS

JGR

Journal of Geophysical Research: Planets

RESEARCH ARTICLE
10.1002/2016JE005025

Key Points:
- Io's atmosphere observed by Gemini-TEXES at 19 μm
- SO_2 band depths drop significantly in Jupiter eclipse
- Modeling indicate primary, molecular atmosphere has collapsed, indicating ice sublimation support

Correspondence to:
C. C. C. Tsang,
con@boulder.swri.edu

Citation:
Tsang, C. C. C., J. R. Spencer, E. Lellouch, M. A. Lopez-Valverde, and M. J. Richter (2016), The collapse of Io's primary atmosphere in Jupiter eclipse, *J. Geophys. Res. Planets*, *121*, 1400–1410, doi:10.1002/2016JE005025.

Received 1 MAR 2016
Accepted 27 MAY 2016
Published online 2 AUG 2016

The collapse of Io's primary atmosphere in Jupiter eclipse

Constantine C. C. Tsang[1], John R. Spencer[1], Emmanuel Lellouch[2], Miguel A. Lopez-Valverde[3], and Matthew J. Richter[4]

[1]Department of Space Studies, Southwest Research Institute, Boulder, Colorado, USA, [2]Observatoire de Paris, LESIA, Meudon, France, [3]Instituto de Astrofisica de Andalucia/CSIC, Granada, Spain, [4]Department of Physics, University of California, Davis, California, USA

Abstract Volcanic outgassing due to tidal heating is the ultimate source of a tenuous SO_2 atmosphere around Jupiter's moon Io. The question of whether SO_2 frost on the surface plays a part, and to what degree, in maintaining Io's atmosphere with the constant volcanic outgassing is still debated. It is believed that for a sublimation-supported atmosphere, the primary atmosphere should collapse during eclipses by Jupiter, as the SO_2 vapor pressure is strongly coupled to the temperature of the ice on the surface. No direct observations of Io's atmosphere in eclipse have previously been possible, due to the simultaneous need for high spectral and time sensitivity, as well as a high signal-to-noise ratio. Here we present the first ever high-resolution spectra at 19 μm of Io's SO_2 atmosphere in Jupiter eclipse from the Gemini telescope. The strongest atmospheric band depth is seen to dramatically decay from 2.5 ± (0.08)% before the eclipse to 0.18 ± (0.16)% after 40 min in eclipse. Further modeling indicates that the atmosphere has collapsed shortly after eclipse ingress, implying that the atmosphere of Io has a strong sublimation-controlled component. The atmospheric column density—from pre-eclipse to in-eclipse—drops by a factor of 5 ± 2.

1. Introduction

Io is host to a spatially inhomogeneous and tenuous atmosphere of neutral SO_2, the ultimate byproduct of extensive and long-lived volcanism on its surface [*Pearl et al*., 1979; *Lellouch*, 1996; *Lellouch et al*., 2007]. The atmosphere is unique in our Solar System for its particular interaction with volcanic plumes and the ice that forms on the surface as a consequence of gas plume condensation. Notable other species from outgassing include SO and NaCl, as well as SO_2 [e.g., *Moullet et al*., 2010].

The exact nature and the mechanisms for supporting this atmosphere are still strongly debated and at times contradictory. The atmospheric density varies with geographic location, with the densest part located on the anti-Jupiter hemisphere, and these variations are larger than diurnal variations [*Jessup and Spencer*, 2015], implying minimal sublimation support. Studies measuring the dependence of a sublimation supported atmosphere with latitude have proved inconclusive [*Feldman et al*., 2000; *Jessup et al*., 2004; *Feaga et al*., 2009]. Although an equator-to-pole decrease in SO_2 density is observed, this can be attributed to more volcanic centers near the equator. Correlations of Io's atmosphere with the positions of volcanoes as well as the longitudinal distribution of SO_2 ice have been equally ambiguous [*Feaga et al*., 2009; *Spencer et al*., 2005]. Observations of far ultraviolet atomic emissions from Io's near-surface and extended atmosphere seem to support the sublimation hypothesis [*Clarke et al*., 1994; *Wolven et al*., 2001; *Retherford et al*., 2007; *Roth et al*., 2011]. A mixture of both sublimation and volcanic support is suggested by a seasonal dependency of the atmospheric density over the Jupiter year [*Tsang et al*., 2012].

If the predominately SO_2 atmosphere is in vapor pressure equilibrium with the large reservoir of SO_2 ice that covers much of Io's surface, as Io enters eclipse and is no longer heated by the Sun, the decreasing surface temperatures will cause the primary atmosphere to collapse out onto the surface [*Saur and Strobel,* 2004]. The atmosphere, with a scale height of 10 km, would transition from a collisionally thick atmosphere, with a mean free path (ι) = 1 m, to an exospheric atmosphere (ι ~100 km). Conversely, if the atmosphere remains constant during eclipse, it would point to a volcanically supported atmosphere. Observations of Io's surface have shown a decrease in its thermal emission during such eclipse events [*Sinton and Kaminski*, 1988]. However, direct observations of the primary atmosphere under eclipse conditions have been difficult to obtain due to the need for spectral resolutions, signal-to-noise ratios (SNR), and time resolutions sufficiently high to resolve the atmosphere's response in eclipse.

Table 1. Observation Log of the Io Eclipse Observations From Gemini-TEXES

Spectrum Number + Phase	Starting Time (UT)	Ending Time (UT)	Middle Time (UT)	Time Relative to Jupiter Eclipse Ingress (min)	Middle Time Io Central Meridian Longitude (°)	Continuum SNR	Air Mass	530.42 cm^{-1} Band Depth (%)
				Date: 17 November 2013				
1 Sunlit	11:02	11:06	11:04	−8.24	340.9	188	1.34	2.22 ± 0.13
2 Sunlit	11:07	11:11	11:09	−3.02	341.6	187	1.32	2.32 ± 0.09
3 Ingress	11:12	11:16	11:14	2.17	342.3	146	1.30	1.92 ± 0.18
4 Eclipse	11:17	11:26	11:21	9.57	343.3	145	1.27	0.94 ± 0.24
5 Eclipse	11:27	11:36	11:31	19.09	344.7	126	1.23	0.59 ± 0.24
6 Eclipse	11:36	11:45	11:40	28.84	345.9	118	1.20	0.06 ± 0.30
7 Eclipse	11:46	11:55	11:50	38.39	347.4	118	1.17	0.60 ± 0.16
8 Eclipse	11:56	12:04	12:00	47.89	349.4	102	1.14	0.17 ± 0.34
				Date: 24 November 2013				
1 Sunlit	12:22	12:27	12:25	−41.33	337.2	385	1.03	2.52 ± 0.07
2 Sunlit	12:28	12:32	12:30	−36.05	337.9	299	1.03	2.44 ± 0.09
3 Sunlit	12:33	12:38	12:35	−30.64	338.6	349	1.03	2.34 ± 0.09
4 Sunlit	12:39	12:43	12:41	−25.00	338.4	359	1.02	2.55 ± 0.08
5 Sunlit	12:44	12:49	12:46	−19.66	340.1	346	1.02	2.30 ± 0.07
6 Sunlit	12:49	12:54	12:51	14.41	340.8	313	1.01	2.59 ± 0.01
7 Sunlit	12:55	13:00	12:57	−8.66	341.7	289	1.01	2.72 ± 0.08
8 Sunlit	13:01	13:03	13:01	−2.00	342.3	354	1.01	2.98 ± 0.01
9 Ingress	13:03	13:06	13:04	1.00	342.7	199	1.01	1.76 ± 0.01
10 Ingress	13:06	13:09	13:07	4.00	343.1	137	1.01	1.73 ± 0.02
11 Eclipse	13:10	13:19	13:14	8.81	344.1	234	1.01	0.67 ± 0.01
12 Eclipse	13:20	13:29	13:24	18.38	345.5	144	1.00	0.37 ± 0.02
13 Eclipse	13:30	13:39	13:34	28.19	346.9	157	1.00	0.42 ± 0.02
14 Eclipse	13:40	13:49	13:44	38.43	348.3	100	1.00	−0.07 ± 0.05
15 Eclipse	13:50	13:58	13:54	47.88	349.7	77	1.01	0.18 ± 0.04

Here we present observations of the primary SO_2 atmosphere of Io as it enters eclipse by Jupiter. The atmosphere appears in absorption at 19 μm, where multiple SO_2 ν_2 vibrational bands exist, most notably a blend of lines near 530.42 cm^{-1} [*Spencer et al.*, 2005; *Tsang et al.*, 2012]. These rotation-vibration lines always appear in absorption as the atmosphere with cold vibrational temperatures is heated from below by a warm surface from a combination of solar heating and heating by volcanoes. The low density of the atmosphere results in longer collisional timescales compared to its radiative timescales, resulting in an atmosphere that is in nonlocal thermodynamical equilibrium (non-LTE) with its kinetic temperature (T_K) [*Lellouch et al.*, 1992]. The observation of the decay of both the atmospheric absorption bands and the thermal flux, before and during eclipse, allows us to elucidate on the nature of the atmosphere in eclipse.

2. Observations

Observations were taken with the 8 m Gemini-north telescope using the Texas Echelon Cross Echelle Spectrograph (TEXES) [*Lacy et al.*, 2002]. These observations occurred over two nights, 17 and 24 November 2013 when Io was at a heliocentric distance of 5.17 AU. The observational details are provided in Table 1. Io was observed during both occasions as it crossed from being sunlit into Jupiter's shadow, from 40 min prior to eclipse ingress to 50 min post-ingress, with high time resolutions between 5 and 10 min per integration. Io subtended 1.1 arc sec in the sky on both nights. TEXES was used in high spectral resolution mode resulting in spectra centered at a wave number of 529.79 cm^{-1} with spectral resolution of approximately 67,000. These settings allowed us to cover seven blended SO_2 absorption features, with gaps in between the echelon grating orders (Figures 1 and 2) at the highest possible spectral resolution in order to resolve the absorption features. The spectrometer slit was placed in the north-south direction on Io, with a length and width of 8 arc sec and 0.75 arc sec, respectively. Targets were nodded along the slit to remove thermal background contributions. The moon Callisto was used as our calibration target due to being spectrally bland in this wavelength range, being brighter than Io, and due to its similar air mass through the observation period: spectra were divided by Callisto to remove telluric and instrumental features. Times and air masses of each spectra on both nights can be found in Table 1. The continuum of all the Io spectra was flattened by taking a number of points in the spectrum that do not have SO_2 absorption and

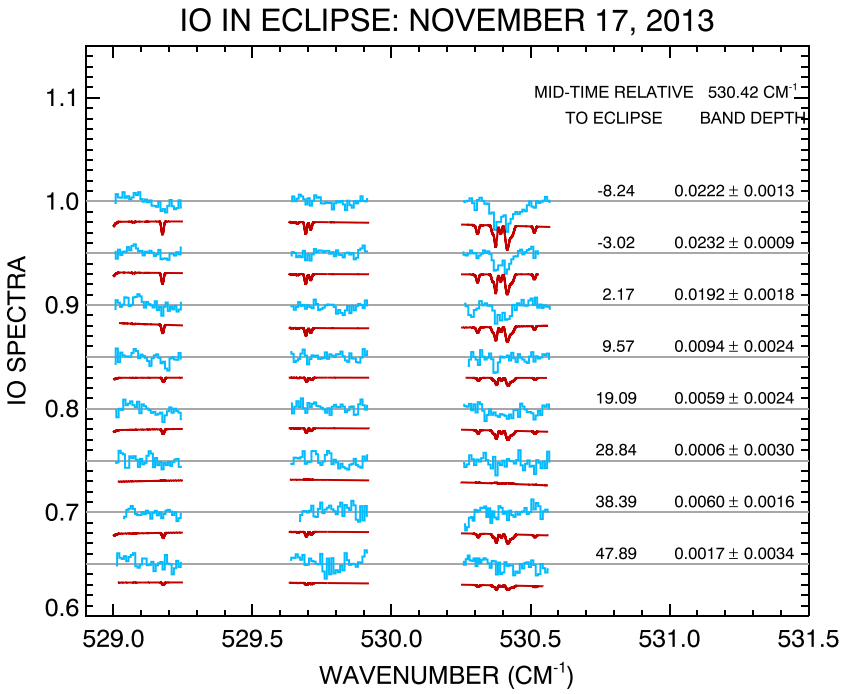

Figure 1. Gemini-TEXES spectra of Io from the 17 November 2013 disappearance event. Observations (blue) are separated between 5 and 10 min, plotted with offsets, and compared to spectra generated by a radiative transfer model (red).

fitting a fourth-order polynomial. This removes any spectral sagging that might be present. Eclipse ingress begins when part of Io's disk enters Jupiter shadow. It takes 4 min for Io to be completely eclipsed by Jupiter. We define the eclipse middle time as the halfway point between Io being fully in sunlight and fully in Jupiter shadow. The observed mid-times are taken from the TEXES data headers, while the time of eclipse ingress is taken from the HORIZONS ephemeris database.

Io's thermal emission at 19 μm drops by a factor of 3.25 (Figure 3) by the end of the observing sequence compared to its flux at start of the eclipse. Some slit loss is expected, but tracking on Io was well maintained on both occasions. Errors in the band depth were determined using a Monte Carlo approach where the measured noise in the spectrum was added to the best fit spectrum and band depths determined again. This process was done 50 times. The depths of the atmospheric absorption features were measured by fitting these observations with a synthetic spectrum generated by a radiative transfer model. All band depths were seen to drop significantly after eclipse ingress for both observations, including the main set of blended lines at 530.42 cm^{-1}, from 2.5 (±0.08)% depth pre-eclipse to 0.18 ± (0.16)% depth after 40 min, a factor of approximately 14 compared to pre-eclipse.

These are the first observations of Io's primary SO_2 atmosphere in Jupiter eclipse and initially, with the measurements of the SO_2 band depths alone, it would seem to indicate a collapsing atmosphere. However, the situation is complicated by the dependence of these band depths with the temperature of the atmosphere and that of the surface. We now begin a thorough analysis to takes these variables into account to arrive at a solution for the atmospheric state in eclipse.

3. Radiative Transfer Model

Synthetic spectra were calculated for the SO_2 ν_2 vibrational bands seen in these 19 μm observations. The radiative transfer model utilizes the Curtis Matrix method and described at length in *López-Puertas and Taylor* [2001] and *López-Valverde and López-Puertas* [1994]. The non-LTE model was used by *Spencer et al.* [2005] and *Tsang et al.* [2012, 2013] to analyze the same SO_2 19 μm (530.42 cm^{-1}) absorption features to look for seasonal effects and longitude variations on Io. The SO_2 line list is provided by HITRAN2K and amended by *Flaud et al.* [1993] and described in *Spencer et al.* [2005]. The Voigt line shape is used, which is valid at these

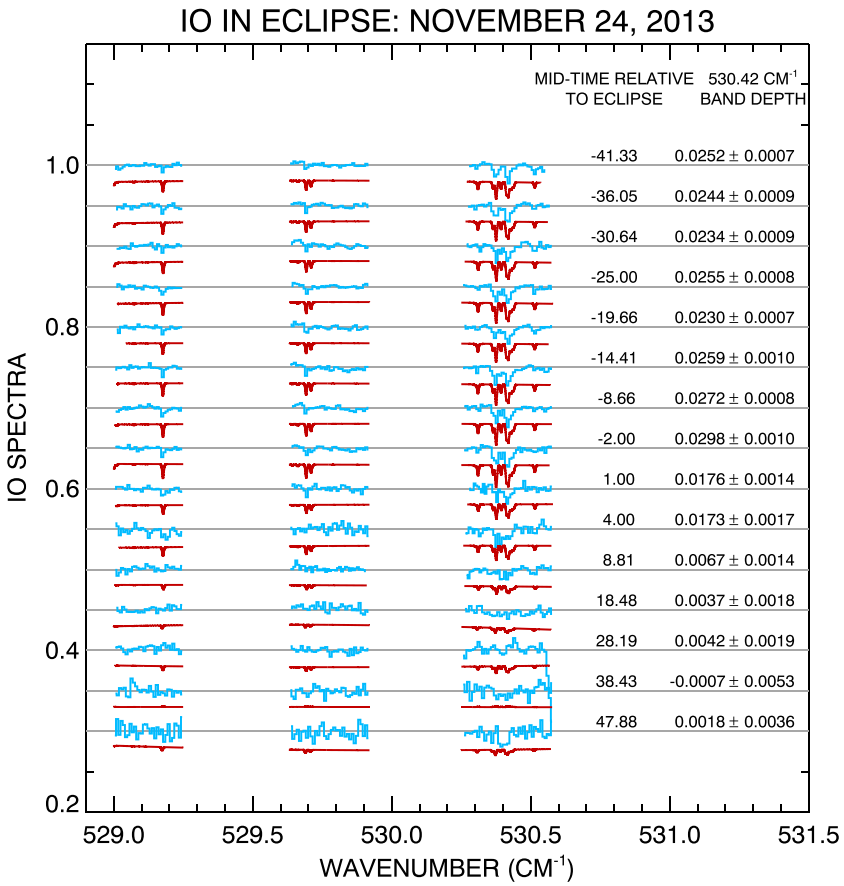

Figure 2. Time resolved Io SO_2 absorption spectra from 529.0 to 530.6 cm^{-1} from Gemini-TEXES. We plot the Gemini-TEXES Io spectra (blue) during eclipse ingress on 24 November 2013. Each spectrum is offset vertically by 0.05. Observations were summed in 5 to 10 min increments at a resolution of ~67,000. The main 530.42 cm^{-1} SO_2 absorption feature can be readily seen prior to eclipse. A radiative transfer model is used to fit for the depth of the absorption feature (red). This and other SO_2 features decrease in strength as the eclipse proceeds.

low densities and far ν_2 line spacings. The radiative transfer model considers the spontaneous and stimulated emission of the (010–000) fundamental band, absorption of upwelling thermal flux from Io's surface and exchanges between layers. The atmospheric vertical temperature profile is assumed to be isothermal. All parameters are spatially invariant. This simplification is reasonable because the retrieved SO_2 column density from the radiative transfer model used here is very similar to the values retrieved for modeled distributions of atmospheric density at these longitudes [*Tsang et al.*, 2013]. Model spectra are calculated from the surface to 200 km in altitude (20 times the scale height of ~10 km) and assume the entire atmosphere is composed of SO_2.

4. Modeling Surface and Atmospheric Temperatures

Previous modeling of the photochemistry and vertical transport of SO_2 in Io's atmosphere showed the radiative timescale of Io's primary atmosphere responding to a change in insolation is ~10^3 s [*Strobel et al.*, 1994]. This is on the same timescale as our observations of SO_2 density (N_{SO2}) in eclipse and much longer than the timescale for sublimation and condensation to affect the SO_2 atmosphere (~100 s, *Summer and Strobel* [1996]), allowing us to study and model the atmospheric response in eclipse. The observed decrease in the SO_2 ν_2 vibrational bands needs to be understood in the context of the changes in surface temperature (T_{SURF}) and atmospheric kinetic temperature (T_{ATM}) before any conclusions of the atmospheric response in eclipse can be made, because band depth depends on these temperatures as well as on column abundance [*Spencer et al.*, 2005; *Tsang et al.*, 2012].

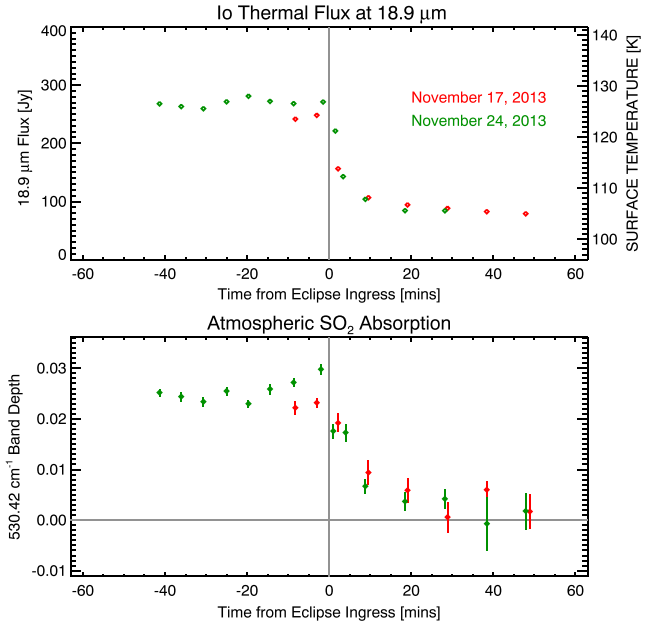

Figure 3. (top) The thermal flux of Io and (bottom) the SO_2 absorption depth at 530.42 cm^{-1} as a function of time relative to Jupiter eclipse. The thermal flux at 19 μm drops by a factor of 3.25 in 30 min as Io cools in eclipse. The atmospheric absorption drops by a factor of ~14 in the same period. The last two flux points on 24 November have been omitted in this plot, as guiding on Io was lost. We use the fluxes from 17 November for those missing flux measurements. The last band depth value on 17 November has been shifted by 1 min for clarity.

4.1. Derivation of T_{SURF}

The width of the TEXES slit at Gemini on Io was 0.75 arc sec, less than Io's 1.1 arc sec diameter. Therefore, Io overfills the slit, and some light loss is expected. The amount of loss depends on guiding and seeing variations. However, the fact that flux varies by less than 2.5% in the 41 min prior to eclipse on 24 November, and the consistency of the absolute fluxes and their variations after eclipse ingress on the two nights (Figure 3), suggests that these variations were modest (with the exception of the last two points on 24 November). We thus have confidence in the relative changes in thermal flux in Figure 3. The last two measurements on 24 November, spanning the last 15 mins, have been omitted due to a loss in guiding on Io. We use the most time appropriate fluxes from 17 November in lieu of these data that span the same time in eclipse.

Note that the TEXES data are not absolutely calibrated in flux. To obtain absolute T_{SURF} in Kelvins, we took previously determined photometric fluxes of Io [*Sinton and Kaminski,* 1988] at 20 μm prior to eclipse ingress (at the same longitudes on Io) and converted those thermal fluxes to a reference wavelength of 19 μm using the Planck function. We then normalized our fluxes and converted them into a brightness temperature using the Planck function. We assume that the brightness temperature is the surface temperature of Io and the majority of the thermal flux is from the passive body of Io that drives ice sublimation. This is reasonable because if the atmosphere was global in extent but the volcanic thermal emissions were significant, the much higher volcanic temperatures (perhaps on the order of ~300 K cf. to the passive surface temperature of ~110 K) would dominate in eclipse. In this limiting case, the SO_2 band depths would therefore increase in eclipse, as the passive emission decreases while the hotter volcanic emissions stay constant. The fact we see the band depths decrease in eclipse requires the atmosphere to have collapsed (as shown in section 5).

4.2. Modeling T_{ATM}

The gas kinetic temperature (T_{ATM}) of SO_2 on Io is poorly known but has a significant effect on the band depths for a given SO_2 column abundance (N_{SO2}). Observations of Io at different wavelengths yield different values for T_{ATM}. Mid-infrared observations at 19 μm tend to produce "cold" atmospheric temperatures (<150 K) [*Spencer et al.*, 2005; *Tsang et al.*, 2012], while recent measurements at 4 μm showed higher gas temperatures (170 ± 20 K) [*Lellouch et al.*, 2015], and this discrepancy remains to be resolved. To estimate T_{ATM} before eclipse ingress, we summed all spectra prior to eclipse ingress from both days (Figures 1 and 2) to create a high-SNR (674 on the continuum and 37 on the depth of the 530.42 cm^{-1} band) spectrum (Figure 4) and fitted for both (N_{SO2}) and (T_{ATM}) using our radiative transfer model. Figure 4 also shows the other numerous SO_2 bands in our spectrum and our ability to fit all bands for N_{SO2} and T_{ATM}. The best fit retrieved N_{SO2} and T_{ATM} was $2.27 \pm (0.3) \times 10^{16}$ cm^{-2} and 115 (−15, +35) K, respectively. The fitting was done with a downhill simplex method for multidimensional chi-square minimization. This low temperature is consistent with previous determinations of T_{ATM} at these wavelengths. We also chose to model an upper limit of T_{ATM} = 170 K as derived at 4 μm data because not only is it a recent and strong constraint on the gas temperature on Io but also it is consistent with the radiative-conductive model of a hydrostatic atmosphere in equilibrium with solar

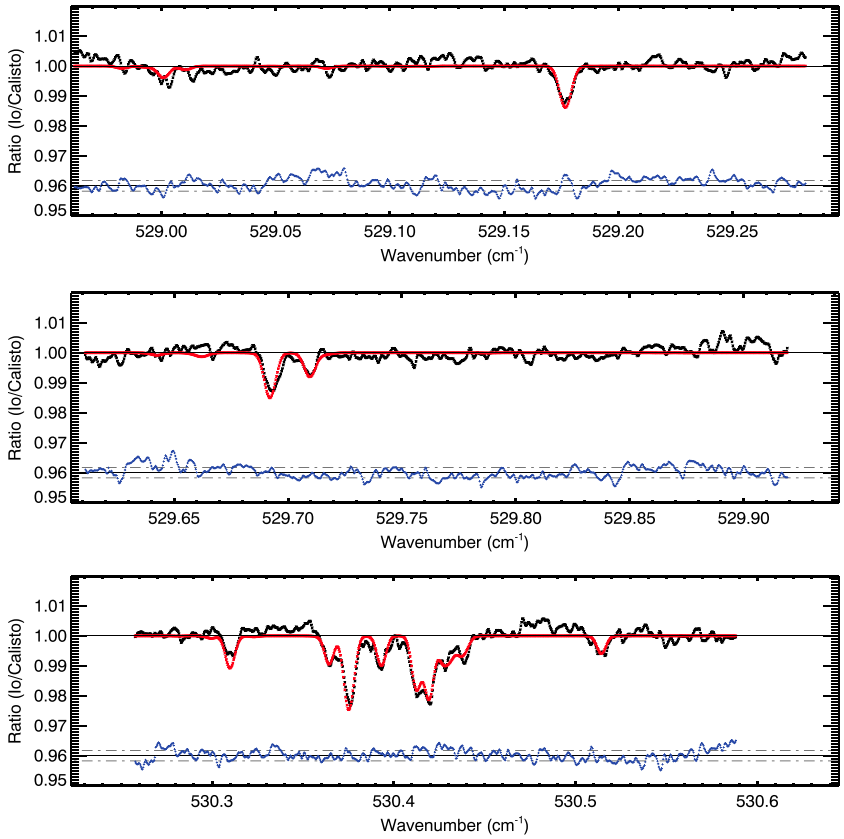

Figure 4. The coadded Gemini-TEXES spectrum from all observations before Jupiter eclipse. All observations from 17 to 23 November 2013 prior to the eclipse ingress were coadded to create this high signal to noise (SNR) (674 on the continuum, 37 on the 530.42 cm^{-1} line) spectrum (black). This spectrum was fitted with a model (red) [*Spencer et al.*, 2005], residuals given in blue, to derive the pre-eclipse T_{ATM}.

heating at these low densities (approximately few nanobars) in the first scale height of Io's atmosphere (~10 km) which these observations probe [*Sinton and Kaminski*, 1988; *Lellouch et al.*, 2015]. With these two initial pre-ingress values of $T_{ATM,}$ we then modeled two end-member scenarios (Figure 5) in which (1) T_{ATM} = constant and (2) T_{ATM}/T_{SURF} is constant. T_{SURF} is derived from the post-eclipse ingress cooling profile by fitting a polynomial function to the values of T_{SURF} inferred above.

5. Results: The Interpretation

For simplicity, we approximate Io as a uniform disk with constant temperature and obtain T_{SURF} from the decrease in the observed 19 μm continuum thermal flux, which was taken at the same time as the SO_2 bands. T_{SURF} was obtained throughout the eclipse period, is a direct measure of surface cooling, and is consistent with previous observations at similar wavelengths [*Sinton and Kaminski*, 1988]. The decrease in 19 μm flux (T_B) is in good agreement on the two dates, indicating that the guiding on Io throughout the eclipse period was accurate and consistent between the dates and changes in observed flux are a good measure of disk-integrated flux changes. This equates to T_{SURF} varying from 127 K out of eclipse [*Sinton and Kaminski*, 1988], cooling to 105 K in eclipse. The pre-eclipse T_{ATM} was measured using a spectrum that was summed from all the pre-eclipse spectra to increase SNR as previously described. The temperature sensitive wing of the main 530.42 cm^{-1} SO_2 line [*Tsang et al.*, 2012], revealed T_{ATM} to be 115 (+35,−15) K, with a best fit SO_2 column density of $N_{SO2} = 2.27 \times 10^{16}$ cm^{-2}. Because an individual spectrum in eclipse did not have sufficient SNR to measure T_{ATM}, we modeled the evolution of T_{ATM} through the eclipse period with two end-member assumptions: either a cooling atmosphere with T_{ATM} in fixed ratio to T_{SURF}, or T_{ATM} constant throughout the eclipse period. Since no observations of T_{ATM} exist, these end-member profiles of T_{ATM} provide good

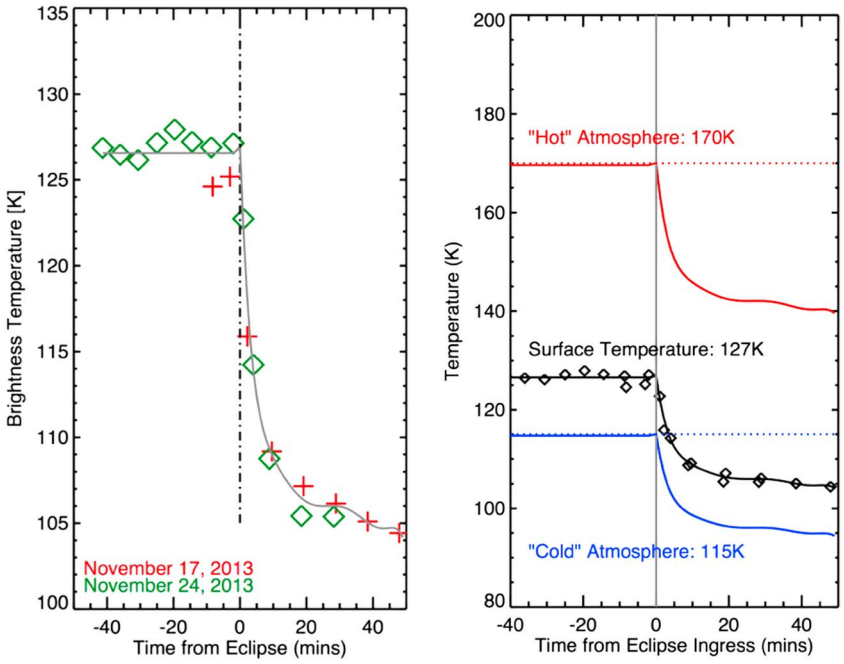

Figure 5. The inferred brightness temperature (T_B) of Io during the observations. The observations in the 19 μm flux are converted to T_B, and a least squares fit is fitted to obtain the time dependent evolution of $T_{SURF}(t)$ (right). The assumed surface temperatures (T_{SURF}) and atmospheric temperatures (T_{ATM}) modeled for the eclipse events.

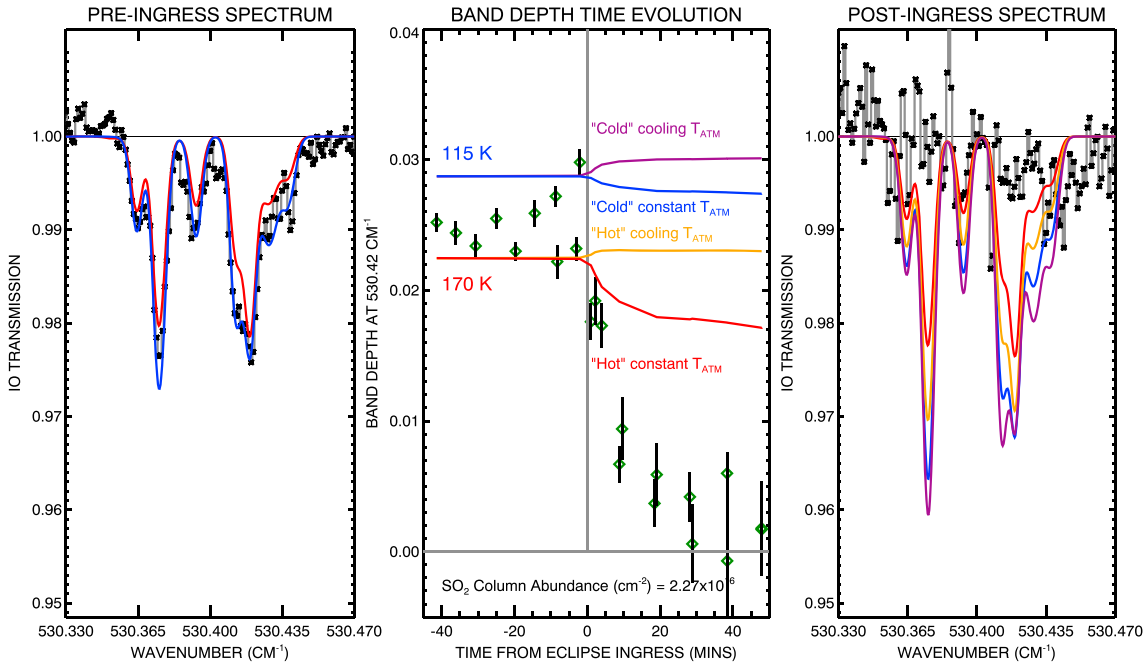

Figure 6. The collapse of Io's atmosphere. Four idealized constant density (static) atmospheres are modeled, with differing starting atmospheric temperatures (T_{ATM}) and assumed temperature behavior in eclipse. The evolution of T_{SURF} is constrained by the observed decay of the 19 μm fluxes (Figure 3). (middle) The 530.42 cm^{-1} band depth for both days has been plotted. Once eclipse occurs, for initial $T_K = 115$ K (blue) and 170 K (red), the atmosphere either cools in fixed proportion to the surface temperature (T_{SURF}) or remains constant, resulting in the band depths presented. (left and right) The average of the first and last 15 min of spectra in Figure 6 (middle), compared with synthetic spectra generated at various T_{ATM} with fixed SO_2 density. These spectra represent end-member behaviors possible on Io for a noncollapsing atmosphere. The observed drop in band depth in eclipse cannot be matched with a constant atmospheric density in any of these models, showing atmospheric collapse has occurred.

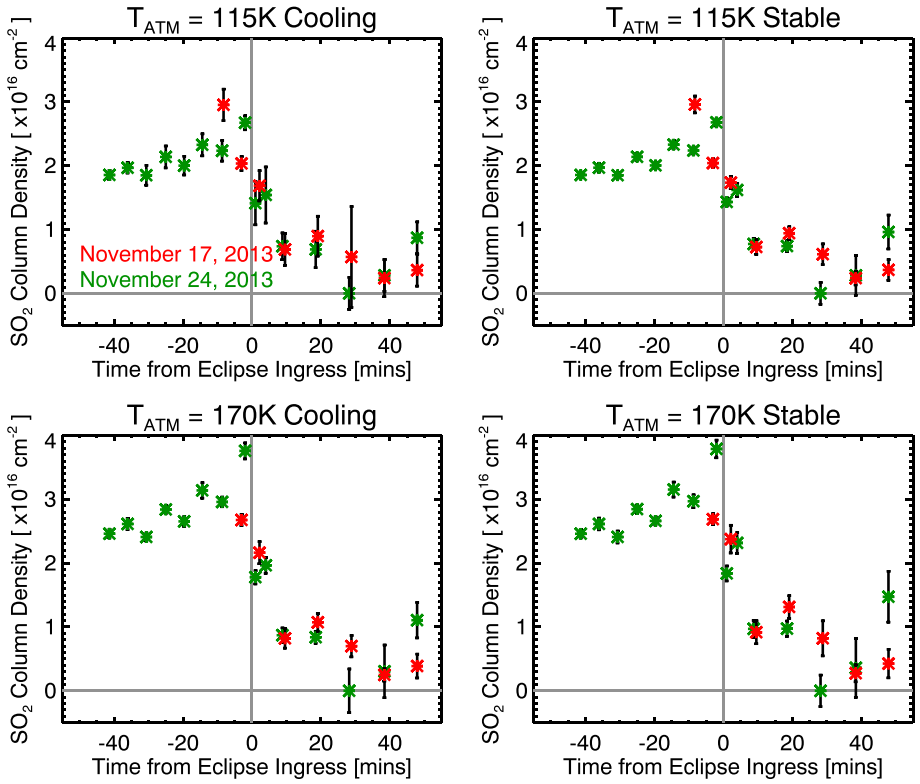

Figure 7. Io's collapsing SO_2 atmosphere during Jupiter eclipse. Inferred atmospheric density before and after eclipse ingress for the four atmospheric temperature models in Figure 3. For all temperature models and both observed eclipses, the best fit SO_2 column abundance (N_{SO2}, cm^{-2}) shows the primary molecular SO_2 atmosphere of Io collapsing during the 40 min following Jupiter eclipse ingress.

boundary conditions to explore the sensitivity of the derived evolution of Io's atmospheric density in eclipse to assumptions about T_{ATM}.

Figure 6 shows the observed 530.420 cm^{-1} band depths (black green) with time, compared to modeled 530.420 cm^{-1} band depths with the above assumptions. We assume a noncollapsing atmosphere with $N_{SO2} = 2.27 \times 10^{16}$ cm^{-2}, an assumed initial atmospheric temperature $T_{ATM} = 115$ K, which is the best fit T_{ATM} from our data and $T_{ATM} = 170$ K which corresponds to the best estimated temperature from *Lellouch et al.* [2015] derived at 4 μm. The constant or cooling atmosphere assumptions are described above, and we use T_{SURF} derived from our disk-integrated Gemini 19 μm fluxes. For both model atmospheres where T_{ATM} is cooling at the same rate as the cooling of T_{SURF}, the 530.420 cm^{-1} band depth post-ingress remains largely unchanged relative to their pre-ingress levels. This is due to a balance between T_{SURF} cooling in the absence of sunlight, which reduces the surface contrast illuminating the overlying atmosphere and produces a decrease in band depth, and T_{ATM} cooling at the same time, which increases the band depths in these low-N_{SO2} non-LTE regimes. For the cases where T_{ATM} = constant, T_{SURF} produces a decrease in band depth as Io cools off in eclipse, but the decrease in both cases is much less than the observed decrease in the N_{SO2} band depths. The observed dramatic drop in band strength thus indicates N_{SO2} must be decreasing in eclipse. We can also derive SO_2 column density given our four assumptions about T_{ATM}. Figure 7 shows the best fit derived N_{SO2} and their errors, assuming the four T_{ATM} evolutions defined already. The tabulation of these values can be found in Table 2.

6. Discussion

These observations provide the first direct evidence that Io's primary molecular SO_2 atmosphere collapses in eclipse, with SO_2 condensing on the surface as SO_2 frost. Our observations also allow us to constrain the

Table 2. The Derived SO_2 Column Densities as a Function of Time From Eclipse Ingress, Assuming T_{ATM} = 115 K or 170 K, Both Either Held Stable and Cooling, Which Is Plotted as Figure 7

	SO_2 Column Density (1×10^{16} cm^{-2})			
Time Relative to Jupiter Eclipse Ingress (min)	T_{ATM} = 115 K Cooling	T_{ATM} = 115 K Stable	T_{ATM} = 170 K Cooling	T_{ATM} = 170 K Stable
−41.33	1.85 ± 0.07	1.85 ± 0.04	2.46 ± 0.07	2.46 ± 0.07
−36.05	1.97 ± 0.08	1.96 ± 0.06	2.61 ± 0.09	2.61 ± 0.09
−30.64	1.85 ± 0.16	1.84 ± 0.05	2.41 ± 0.06	2.41 ± 0.09
−25.00	2.14 ± 0.17	2.13 ± 0.05	2.84 ± 0.06	2.85 ± 0.07
−19.66	2.00 ± 0.15	2.00 ± 0.05	2.65 ± 0.08	2.66 ± 0.06
−14.41	2.33 ± 0.17	2.33 ± 0.06	3.14 ± 0.12	3.15 ± 0.12
−8.66	2.23 ± 0.16	2.24 ± 0.05	2.96 ± 0.08	2.97 ± 0.10
−8.24	2.95 ± 0.25	2.96 ± 0.13	4.33 ± 0.22	4.36 ± 0.19
−3.02	2.03 ± 0.11	2.04 ± 0.06	2.68 ± 0.09	2.69 ± 0.09
−2.00	2.67 ± 0.11	2.67 ± 0.05	3.76 ± 0.13	3.79 ± 0.14
1.00	1.41 ± 0.34	1.43 ± 0.06	1.78 ± 0.10	1.84 ± 0.12
2.17	1.69 ± 0.24	1.73 ± 0.09	2.16 ± 0.17	2.38 ± 0.22
4.00	1.54 ± 0.44	1.61 ± 0.10	1.96 ± 0.12	2.32 ± 0.16
8.81	0.74 ± 0.21	0.77 ± 0.08	0.87 ± 0.11	0.97 ± 0.13
9.57	0.69 ± 0.25	0.72 ± 0.11	0.82 ± 0.15	0.92 ± 0.18
18.48	0.69 ± 0.28	0.74 ± 0.08	0.84 ± 0.09	0.97 ± 0.12
19.09	0.90 ± 0.31	0.94 ± 0.10	1.07 ± 0.14	1.31 ± 0.18
28.19	0.00 ± 0.93	0.02 ± 0.17	0.00 ± 0.34	0.00 ± 0.25
28.84	0.57 ± 0.79	0.61 ± 0.16	0.70 ± 0.17	0.82 ± 0.27
38.39	0.24 ± 0.29	0.23 ± 0.10	0.25 ± 0.10	0.27 ± 0.13
38.43	0.28 ± 0.31	0.28 ± 0.30	0.30 ± 0.41	0.36 ± 0.46
47.88	0.87 ± 0.36	0.96 ± 0.26	1.11 ± 0.28	1.47 ± 0.40
47.89	0.36 ± 0.30	0.36 ± 0.17	0.39 ± 0.19	0.43 ± 0.22

spatial distribution of Io's atmosphere. The fact that these observations show SO_2 band depths decreasing until they almost disappear implies the atmosphere, at least on the hemisphere centered around 340° that is observed during eclipses, is global and not centered over volcanic hotspots; i.e., localized SO_2 over active volcanoes is a minor component of the atmosphere on this hemisphere. A single high value in SO_2 column density on 24 November just prior to eclipse gives the impression of a rise in column density before the collapse begins. This value is unlikely to be as high as indicated as the atmospheric density has no physical reason to increase prior to eclipse ingress.

In apparent contradiction to the conclusions of this study, recent mid-UV observations by the Hubble Space Telescope have suggested Io's atmosphere coming out of Jupiter eclipse does not rapidly respond to sunlight, as expected if the atmosphere was sublimation supported [*Tsang et al.*, 2015], as evidence by this work. One possible explanation of the difference could be longitudinal variations in atmospheric support. Multiwavelength observations [*Spencer et al.*, 2005; *Feaga et al.*, 2009; *Tsang et al.*, 2013] show the atmospheric density peaks at anti-Jupiter longitudes (~180°W) and decreases toward the sub-Jupiter hemisphere. The atmospheric densities at eclipse ingress longitudes (~340°W) are a factor of 2 lower than at eclipse egress longitudes (20°W) [*Tsang et al.*, 2012, 2013]. Egress longitudes also contain ~40% more volcanically active hotspots and paterae than at ingress longitudes as seen by the Galileo spacecraft [*Feaga et al.*, 2009; *Hamilton et al.*, 2013]. We postulate that at ingress longitudes, the atmosphere is dominated by ice sublimation, but at egress longitudes where the atmosphere is twice as thick, SO_2 emission from the larger number of volcanoes largely masks the sublimation response to sunlight. Further modeling and observations are needed to confirm both these observations and resolve this discrepancy.

Lastly, sulfur monoxide (SO), which has been detected on Io [*de Pater et al.*, 2002] is a noncondensable at Io temperatures. It has been suggested that SO might potentially inhibit any condensing SO_2 onto the surface by forming a thick diffusion layer [*Moore et al.*, 2009] between the surface and the SO_2 atmosphere, as the SO diffusion coefficient is inversely proportional to the SO_2 density. However, at the surface, SO recombines into S_2O and SO_2. Laboratory experiments that attempt to measure the vapor pressure expression of SO show that this fast reaction scheme prevents SO from remaining long enough to measure its vapor pressure

[*Lellouch et al*., 1996]. Therefore, the SO "atmosphere" should collapse with the SO_2 atmosphere. The fact that we see the atmosphere collapse shows that any noncondensables such as SO do not affect the collapsing mechanism, as suggested by these laboratory measurements.

7. Conclusions

We used the Gemini North telescope to obtain data of Io's molecular SO_2 atmosphere during Io's eclipse ingress. Spectra were taken by the TEXES spectrometer at 530.42 cm^{-1} (19 μm) on two separate ingress apparitions in 2013, at resolving powers of 67,000. The data and analysis show for the first time that the primary atmosphere of Io collapsed shortly after eclipse ingress. Our main conclusions are the following:

1. The main 530.420 cm^{-1} SO_2 band depths was observed to decay away in the period of Jupiter eclipse, from 2.5 ± (0.08)% before the eclipse to 0.18 ± (0.16)% after 40 min in eclipse. It was also accompanied by a drop in 19 μm thermal flux, equating to a drop in the brightness temperature from 127 K to 105 K.
2. Modeling shows that for end-member atmospheric temperatures of 115 K and 170 K that are most likely found on Io, the SO_2 band depths cannot be reconciled with an atmosphere that is static in time and which does not respond to sunlight.
3. The atmospheric density drop according to the vapor pressure laws imply a decrease from 2.0–2.5 × 10^{16} cm^{-2} to ~0.5 × 10^{16} cm^{-2} to match the observed drop in band depths. The atmosphere collapses by a factor of 5 ± 2.
4. Combined with the HST-COS egress UV observations taken a few years prior, we can infer that the atmosphere at ingress longitudes are mostly sublimation driven, while at egress longitudes, the atmosphere is mostly volcanically dominated. This agrees with the distribution of atmospheric density with longitudes, as well as the distribution of volcanic centers found on Io. The data also show that the effect of any noncondensable gases is negligible.

Acknowledgments

C.C.C.T. and J.R.S. at Southwest Research Institute were funded by NASA Outer Planets Research grant NNX14AC63G and Planetary Astronomy grant NNX11AD61G. M.A.L.V. was funded by the Spanish Ministerio de Economia y Competitividad and by FEDER funds under project ESP2015-65064-C2-1-P (MINECO/FEDER) We thank Darrel Strobel and one anonymous reviewer for their comments that improved the quality of this paper. Please contact the corresponding author, Constantine Tsang, at con@boulder.swri.edu regarding access to the data. The observational data and derived data products are available at the authors website repository: http://www.boulder.swri.edu/~con/Site/Data_Gem.html. Based on observations obtained at the Gemini Observatory, which is operated by the Association of Universities for Research in Astronomy, Inc., under a cooperative agreement with the NSF on behalf of the Gemini partnership: the National Science Foundation (United States), the National Research Council (Canada), CONICYT (Chile), Ministerio de Ciencia, Tecnología e Innovación Productiva (Argentina), and Ministério da Ciência, Tecnologia e Inovação (Brazil). We thank the Gemini Observatory and the U.S. National Gemini Office for their support and assistance with making TEXES available to the Gemini community.

References

Clarke, J. T., J. Ajello, J. Luhmann, N. Schneider, and I. Kanik (1994), Hubble Space Telescope UV spectral observations of Io passing into eclipse, *J. Geophys. Res.*, *99*(E4), 8387–8402.

de Pater, I., H. Roe, J. R. Graham, D. F. Strobel, and P. Bernath (2002), Detection of the forbidden SO rovibronic transition on Io at 1.7 mm, *Icarus*, *156*, 296–301.

Feaga, L. M., M. McGrath, and P. D. Feldman (2009), Io's dayside SO_2 atmosphere, *Icarus*, *201*, 570–584.

Feldman, P. D., D. F. Strobel, H. W. Moos, K. D. Retherford, B. C. Wolven, M. A. McGrath, F. L. Roesler, R. C. Woodward, R. J. Oliversen, and G. E. Ballester (2000), Lyman-alpha imaging of the SO_2 distribution on Io, *Geophys. Res. Lett.*, *27*, 1787–1789, doi:10.1029/1999GL011067.

Flaud, J.-M., A. Perrin, L. M. Salah, W. J. Lafferty, and G. Guelachvili (1993), A reanalysis of the (010), (020), (100), and (001) rotational levels of $32S16O_2$, *J. Mol. Spectrosc.*, *160*, 272–278.

Hamilton, C. W., C. D. Beggan, S. Still, M. Beuthe, R. M. C. Lopes, D. A. Williams, J. Radebaugh, and W. Wright (2013), Spatial distribution of volcanoes on Io: Implications for tidal heating and magma ascent, *Earth Planet. Sci. Lett.*, *361*, 272–286.

Jessup, K.-L., and J. R. Spencer (2015), Spatially resolved HST/STIS observations of Io's dayside equatorial atmosphere, *Icarus*, *248*, 165–189, doi:10.1016/j.icarus.2014.10.020.

Jessup, K. L., J. R. Spencer, G. E. Ballester, R. R. Howell, F. Roesler, M. Vigil, and R. Yelle (2004), The atmospheric signature of Io's Prometheus plume and anti-Jovian hemisphere: Evidence for a sublimation atmosphere, *Icarus*, *169*, 197–215.

Lacy, J. H., M. J. Ritcher, T. K. Greathouse, D. T. Jaffe, and Q. Zhu (2002), TEXES: A sensitive high-resolution grating spectrograph for the mid-infrared, *Pub. Astro. Soc. Pacific*, *114*, 153–168.

Lellouch, E. (1996), Io's Atmosphere, *Not Yet Understood*, *124*, 1–21.

Lellouch, E., M. J. S. Belton, I. DePater, G. Paubert, S. Gulkis, and T. Encrenaz (1992), The structure, stability, and global distribution of Io's atmosphere, *Icarus*, *98*, 271–295.

Lellouch, E., D. F. Strobel, M. J. S. Belton, M. E. Summers, G. Paubert, and R. Moreno (1996), Detection of sulfur monoxide in Io's atmosphere, *Astrophy. J.*, *459*, L107–L110.

Lellouch, E., M. A. McGrath, and K. L. Jessup (2007), Io's atmosphere, in *Io After Galileo*, edited by R. M. C. Lopes and J. R. Spencer, pp. 231–264, Springer, Praxis.

Lellouch, E., M. Ali-Dib, K.-L. Jessup, A. Smette, H.-U. Käufl, and F. Marchis (2015), Detection and characterization of Io's atmosphere from high-resolution 4-μm spectroscopy, *Icarus*, *253*, 99–114, doi:10.1016/j.icarus.2015.02.018.

López-Puertas, M., and F. W. Taylor (2001), *Non-LTE Radiative Transfer in the Atmosphere*, World Sci., Singapore.

López-Valverde, M. A., and M. López-Puertas (1994), A non-local thermodynamic equilibrium radiative transfer model for infrared emissions in the atmosphere of Mars: 1. Theoretical basis and nighttime populations of vibrational levels, *J. Geophys. Res.*, *99*, 13,093–13,116, doi:10.1029/94JE00635.

Moore, C. H., D. B. Goldstein, P. L. Varghese, L. M. Trafton, and B. Stewart (2009), 1-D DSMC simulation of Io's atmospheric collapse and reformation during and after eclipse, *Icarus*, *201*, 585–597.

Moullet, A., M. A. Gurwell, E. Lellouch, and R. Moreno (2010), Simultaneous mapping SO_2, SO, NaCl in Io's atmosphere with the submillimeter array, *Icarus*, *208*, 353–365.

Pearl, J., R. Hanel, V. Kunde, W. Maguire, K. Fox, S. Gupta, C. Ponnamperuma, and F. Raulin (1979), Identification of gaseous SO_2 and new upper limits for other gases on Io, *Nature*, *280*, 755–758.

Retherford, K., et al. (2007), Io's atmospheric response to eclipse: UV aurorae observations, *Science*, *318*, 237–240.
Roth, L., J. Saur, K. D. Retherford, D. F. Strobel, and J. R. Spencer (2011), Simulation of Io's auroral emission: Constraints on the atmosphere in eclipse, *Icarus*, *214*, 495–509.
Saur, J., and D. F. Strobel (2004), Relative contributions of sublimation and volcanos to Io's atmosphere inferred from its plasma interaction during solar eclipse, *Icarus*, *171*, 411–420.
Sinton, W., and C. Kaminski (1988), Infrared observations of eclipses of Io, its thermophysical parameters and the thermal radiation of the Loki Volcano and Environs, *Icarus*, *75*, 207–232.
Summer, M. E., and D. F. Strobel (1996), Photochemistry and vertical transport in Io's atmosphere and ionosphere, *Icarus*, *120*, 290–316.
Spencer, J. R., E. Lellouch, M. J. Richter, M. A. López-Valverde, K. L. Jessup, T. K. Greathouse, and J. M. Flaud (2005), Mid-infrared detection of large longitudinal asymmetries in Io's SO_2 atmosphere, *Icarus*, *176*, 283–304.
Strobel, D. F., X. Zhu, and M. E. Summers (1994), On the vertical thermal structure of Io's atmosphere, *Icarus*, *111*, 18–30.
Tsang, C. C. C., J. R. Spencer, E. Lellouch, M. A. Lopez-Valverde, M. J. Richter, and T. K. Greathouse (2012), Io's atmosphere: Constraints on sublimation support from density variations on seasonal timescales using NASA IRTF/TEXES observations from 2001 to 2010, *Icarus*, *217*, 277–296.
Tsang, C. C. C., J. R. Spencer, and K. L. Jessup (2013), Synergistic observations of Io's atmosphere in 2010 from HST-COS in the mid-ultraviolet and IRTF-TEXES in the mid-infrared, *Icarus*, *226*, 604–616.
Tsang, C. C. C., J. R. Spencer, and K.-L. Jessup (2015), Non-detection of post-eclipse changes in Io's Jupiter-facing atmosphere: Evidence for volcanic support?, *Icarus*, *248*, 243–253, doi:10.1016/j.icarus.2014.10.033.
Wolven, B. C., H. W. Moos, K. D. Retherford, P. D. Feldman, D. F. Strobel, W. H. Smyth, and F. L. Roesler (2001), Emission profile of neutral oxygen and sulfur in Io's exospheric corona, *J. Geophys. Res.*, *106*(A11), 26,155–26,182.